



AMERICAN METEOROLOGICAL SOCIETY

Journal of Atmospheric and Oceanic Technology

EARLY ONLINE RELEASE

This is a preliminary PDF of the author-produced manuscript that has been peer-reviewed and accepted for publication. Since it is being posted so soon after acceptance, it has not yet been copyedited, formatted, or processed by AMS Publications. This preliminary version of the manuscript may be downloaded, distributed, and cited, but please be aware that there will be visual differences and possibly some content differences between this version and the final published version.

The DOI for this manuscript is doi: [10.1175/JTECH-D-10-05043.1](https://doi.org/10.1175/JTECH-D-10-05043.1)

The final published version of this manuscript will replace the preliminary version at the above DOI once it is available.



**Comparison between the TOPAZ airborne ozone lidar and in situ measurements
during TexAQS 2006**

A.O. Langford¹, C.J. Senff^{1,2}, R.J. Alvarez¹ II, R.M. Banta¹, R.M. Hardesty¹, D.D.
Parrish¹, T.B. Ryerson¹

¹Chemical Sciences Division, Earth System Research Laboratory,
NOAA, Boulder, Colorado, USA

²Cooperative Institute for Research in Environmental Sciences,
University of Colorado, Boulder, and Chemical Sciences Division,
Earth System Research Laboratory, NOAA, Boulder, Colorado, USA

submitted to J. Oceanic Atmos. Tech

December 6, 2010

Revised March 31, 2011

Corresponding author: Andrew O. Langford, NOAA Earth System Research Laboratory,
325 Broadway, R/CSD3, Boulder, CO 80305, USA. (andrew.o.langford@noaa.gov)

ABSTRACT

The NOAA airborne ozone lidar system (TOPAZ) is compared with the fast response chemiluminescence sensor flown aboard the NOAA WP-3D during TexAQS 2006. TOPAZ measurements made from the NOAA Twin Otter flying at an altitude of ~3300 m MSL in the Houston area on 31 August, and the Dallas area on 13 September, show that the overall uncertainty in the 10-s (~600 m horizontal resolution) TOPAZ profiles is dominated by statistical uncertainties (1σ) of ~ 8 ppbv (6-10%) at ranges of ~2300 m from the aircraft (~1000 m MSL), and ~11-27 ppbv (12-30%) at ranges of ~2800 m (~500 m MSL). These uncertainties are substantially reduced by spatial averaging, and the averages of 11 profiles (110-s or 6.6 km horizontal resolution) at ~1000 m MSL are in excellent agreement ($\pm 2\%$) with the in situ measurements at ~500 m MSL. The TOPAZ measurements at lower altitudes on 31 August exhibit a negative bias of up to ~15%, however, when the lidar signals were strongly attenuated by very high ozone levels in the plume from the Houston Ship Channel. This bias appears to result from nonlinear behavior in the TOPAZ signal amplifiers described in the companion paper by Alvarez et al. (2011). An empirical correction is presented.

1. Introduction

Tropospheric ozone (O_3) is a harmful secondary pollutant (U.S. Environmental Protection Agency 2006) and a potent greenhouse gas (Forster et al. 2007) derived primarily from photochemical reactions of NO_x and volatile organic compounds (VOCs) released from natural and anthropogenic sources at the Earth's surface (Horowitz 2006). Some ozone is also transported from the lower stratosphere into the troposphere (Langford and Reid 1998) where it occasionally causes noticeable enhancements in surface ozone (Langford et al. 2009a). Conversely, some anthropogenic ozone can be transported from the boundary layer into the free troposphere (Langford et al. 2010a,b) where it has a larger radiative impact (Forster et al. 1996) and can influence air quality far from source regions (Cooper et al. 2010; Parrish et al. 1993). A better understanding of the processes influencing the spatial distribution and temporal variability of ozone in the boundary layer and free troposphere is needed to formulate strategies for improving air quality and stabilizing the Earth's radiative balance.

Many techniques are used to measure tropospheric ozone. Satellite-based sensors measure the spatial distribution over a wide geographic area, but with limited temporal coverage and poor horizontal and vertical resolution (Munro et al. 1998). Ozonesondes provide good vertical resolution, but only from a fixed location and with limited temporal coverage (Newchurch et al. 2003). Ground-based differential absorption lidar (DIAL) offers better temporal coverage, but also has limited spatial coverage (Machol et al. 2009). Although each of these techniques fills an important measurement niche, none provides high spatial and temporal resolution along with the coverage needed for detailed studies of ozone production and transport in the boundary layer and lower free

troposphere. For these types of studies, in situ monitors aboard research aircraft provide the most accurate and precise measurements. These monitors are also typically flown with a suite of other instruments to give a detailed picture of the chemistry controlling ozone production and destruction (Ryerson et al. 2001). However, in situ monitors measure the concentration only within the volume directly accessed by the aircraft platform and give an incomplete picture of the transport processes that contribute to the observed variations. Airborne DIAL can help to fill this gap by measuring ozone below and/or above the aircraft with better spatial coverage than ozonesondes or ground-based DIAL, and with higher accuracy and better range resolution than satellite retrievals. Airborne DIAL has long been used to map out ozone distributions near stratospheric intrusions and in the free troposphere (Browell et al. 1983), and more recently in plumes from urban areas (Banta et al. 2005) or power plants (Senff et al. 1998). However, as with all measurement techniques, interpretation of the results requires a good understanding of the measurement uncertainties and limitations.

The Chemical Science Division of the National Oceanic and Atmospheric Administration Earth System Research Laboratory (NOAA ESRL/CSD) recently developed a compact downward-looking ozone DIAL system based on a tunable solid-state laser for operation on small aircraft such as the NOAA Twin Otter. This instrument, the Tunable Optical Profiler for Aerosol and oZone (TOPAZ), was deployed during the TexAQS 2006 field campaign (Senff et al. 2010) and the Pre-CalNex field campaign in 2009 (Langford et al. 2010a). TOPAZ replaces a larger excimer laser-based system originally developed at the U.S. Environmental Protection Agency (EPA) (Kovalev and McElroy 1994) and deployed during the Nashville SOS studies in 1995 (Alvarez et al.

1998; Banta et al. 1998; Senff et al. 1998) and 1999, the first TexAQS study in 2000 (Banta et al. 2005), and NEAQS-ICARTT in 2004. Details of the TOPAZ hardware, methodology, and analysis are described in the companion paper (Alvarez et al. 2011). Here, we compare TOPAZ measurements made during the TexAQS 2006 study with in situ measurements from the chemiluminescence monitor (Ryerson et al. 1998) flown aboard the NOAA WP-3D. We use these comparisons to assess the overall uncertainty of the TOPAZ measurements and identify the factors influencing the measurement accuracy and precision.

2. Data and analysis

The field intensive portion of the second Texas Air Quality Study and the Gulf of Mexico Atmospheric Composition and Climate Study (TexAQS/GoMACCS) took place in eastern Texas and the nearby Gulf of Mexico from August to October 2006. The NOAA WP-3D and Twin Otter aircraft combined with the R/V Ronald H. Brown, the Radar Wind Profiler Network, and surface measurement networks to conduct the joint study. Many of the study findings are described in a special section of the *Journal of Geophysical Research* (Parrish et al. 2009). In situ ozone measurements were made from the WP-3D during the study with an ozone monitor based on the NO-induced chemiluminescence technique (Ridley et al. 1992). This instrument has been extensively tested (Ryerson et al. 1998) and has a nominal accuracy of 3% and a precision of ± 0.05 ppbv for a sample time of 1 s (Parrish et al. 2009). The 1-s sample time and WP-3D ground speed of $\sim 100 \text{ m s}^{-1}$ give a typical horizontal resolution of $\sim 100 \text{ m}$. TOPAZ was operated from the Twin Otter during TexAQS 2006 and the data were processed as

described by Alvarez et al. (2011). Briefly, the archived 1-s backscatter return signals from near and far range channels were combined and empirically corrected for signal-induced bias (SIB) and amplifier overshoot. These corrected signals were then integrated for 10 s. Ozone number density profiles were calculated from the 10-s signals with a range resolution of 90 m and converted to concentration profiles using temperature and pressure profiles from the NCEP Reanalysis (Kalnay et al. 1996). These profiles were smoothed over five running gates (450 m) to reduce the statistical noise. The 10-s averaging time and mean Twin Otter ground speed of $\sim 60 \text{ m s}^{-1}$ give a maximum horizontal resolution of $\sim 600 \text{ m}$. Both the WP-3D in situ and TOPAZ measurements used in this paper are the versions archived at the NOAA Tropospheric Chemistry website (<http://www.esrl.noaa.gov/csd/tropchem/>). These version 2 data have been used in several recent studies of ozone production and transport during TexAQS 2006 (Banta et al. 2011; Langford et al. 2009b; Langford et al. 2010b; Senff et al. 2010).

3. Results and Analysis

The Twin Otter flew 22 missions during TexAQS 2006 totaling about 121 hours between 1 August and 13 September, covering the Houston, Dallas/Fort Worth, and eastern Texas areas. The WP-3D flew from Tampa, FL to Houston on 31 August, but was subsequently grounded until 11 September for repairs. The WP-3D then flew 16 missions between 11 September and 12 October. Coordinated measurements were therefore possible only on 31 August and 13 September, and then only with the WP-3D flying at a constant altitude of $\sim 500 \text{ m MSL}$. Nevertheless, the measurements made on these two days sampled a wide range of conditions and are the basis for this study.

a. High ozone: Houston, 31 August

The flights on 31 August coincided with the second highest hourly mean surface ozone concentrations (147 ppbv) recorded by the Texas Commission on Environmental Quality (TCEQ) Continuous Ambient Monitoring Station (CAMS) network in Houston during the month of August, and the highest 8-h mean ozone concentrations (126 ppbv) recorded during all of 2006 (Langford et al. 2009b). The ambient conditions on this day thus represent some of the highest ozone concentrations likely to be encountered within the continental United States (Kleinman et al. 2002). PM_{2.5} levels were also elevated, but remained in the “moderate” EPA Air Quality Index (AQI) range.

The 5-min CAMS surface measurements from 2100 UTC on 31 August (Fig. 1a) show a plume of high ozone emanating from the Houston Ship Channel. This plume was advected westward by the (Galveston) Bay breeze and rotated to the north by the Gulf breeze (cf. Banta et al. 2005). The Twin Otter flight plan was modified after take off to intercept this plume, and followed a grid pattern extending westward from 29.75°N, 94.6°W. This pattern, represented by the solid blue line in Fig. 1a, transected the ozone plume six times. TOPAZ acquired 1678 10-s ozone profiles between 1759 and 2238 UTC (1159 to 1638 LST). The Twin Otter descended from ~3400 m MSL to 3075 m MSL at 2107 UTC (blue line in Fig. 1b) to avoid scattered clouds to the northwest of downtown Houston. The WP-3D arrived in Houston from Tampa during the early afternoon, approaching from the east at ~500 m MSL along latitude 29.80°N (red lines in Figs. 1a and 1b). The WP-3D passed through the ozone plume before turning south at 96.0°W. The aircraft then turned eastward at 29.41°N, flying to the south of the plume,

before turning to the southeast at $\sim 94.8^\circ\text{W}$. The WP-3D then climbed to nearly 3700 m MSL over the Gulf of Mexico before returning to Houston and landing.

The WP-3D flight path intersected or overlapped the Twin Otter flight pattern on 16 occasions between 2015 and 2115 UTC (cf. Fig. 1a). These points are labeled with the letters A through P (in order of WP-3D flight time). Since the Twin Otter flew more slowly and executed a more complex flight pattern, it crossed these waypoints as long as 93 minutes before, and 144 minutes after the WP-3D. The dashed boxes in Fig. 1a enclose the nine waypoints labeled with black letters that were crossed by both aircraft within a time window of ± 60 min. The measurements within these boxes, which are represented by overlapping blue and red solid rectangles, will be examined in detail below, together with the measurements along the two transects (GJ and HI) enclosed by the dotted rectangles. The orange circles represent those CAMS sites nearest to the waypoints that lie within the 6 x 6 km dashed boxes.

Figure 2a shows a curtain plot of the TOPAZ measurements made over the northbound flight leg within the dotted rectangle enclosing points G and J in Fig. 1a. This transect crossed the western edge of the ozone plume, where TOPAZ measured concentrations of up to 168 ± 8 ppbv at 1270 m MSL near point G. The maximum ozone concentrations ~ 45 km to the south near point J are much lower, ~ 80 -90 ppbv. The solid black line shows the altitude of the peak gradient in aerosol backscatter identified using a Haar wavelet technique (Senff et al. 2010). This altitude coincides with the top of the convective boundary layer on most days (White et al. 1999). However, a stable capping layer with strong northerly winds associated with a deep upper-level trough limited convective mixing to less than 1200 m MSL over much of the Houston area on the 31st,

particularly to the south of downtown (Langford et al. 2010b). Figure 2a shows that along some flight legs the plume was modulated by gravity waves created when rising convective cells impinged on this layer (Kuettnner et al. 1987). The plume was also lifted above the mixed layer by low-level convergence along the sea breeze front and spread to the south by strong northerly winds associated with the upper-level trough. This is more obvious in Fig. 2b, which plots the data from the southbound flight leg within the dotted rectangle enclosing points H and I. The ozone concentrations are generally much lower along this transect, but the plume is still evident near H. The WP-3D flight track intersects the curtain plot in Fig. 2a at the open squares labeled G and J; these have been color-coded using the in situ measurements with the same color scale as the TOPAZ measurements. The rectangular box in Fig. 2b encloses the nearly collocated in situ measurements along the H-I transect.

Figure 2 shows that there is good agreement between the lidar and in situ measurements within the resolution of the contour color scheme. Closer examination of the data exposes some quantitative differences, however. Figure 3a shows the area surrounding point J in more detail. These measurements were the most nearly coincident in time (~ 3 min), and both instruments should have sampled nearly the same airmass. The dashed box encloses a 6×6 km ($\sim 0.06^\circ \times 0.06^\circ$) footprint around the waypoint. The blue squares mark the centers of the 11 (10-s) TOPAZ profiles, and the overlapping red squares the 51 (1-s) in situ measurements within this window. The TOPAZ and in situ measurements are plotted in Fig. 3b as a function of altitude. The dotted blue lines show the 10-s TOPAZ profiles corresponding to the blue squares in Fig. 3a. The heavy black line shows the mean of these profiles with error bars representing the standard deviations

of the mean at the center of each 90-m DIAL range gate. The red squares represent the (1-s) WP-3D in situ data within the box in Fig. 3a. The green line shows the mean of the corresponding 11 (10-s) aerosol backscatter profiles. The aerosol backscatter changes little with altitude below ~950 m MSL, which provides a lower limit for the top of the local mixing layer. Only a lower limit can be established since relative humidity increases with altitude in the convective mixing layer and the backscatter will also increase if the aerosol particles absorb water and grow. The heavy dashed blue line near the left axis shows the ozone error due to differential aerosol scattering (Alvarez et al. 2011). This error is always less than 0.5 ppbv below 1000 m MSL, and less than 3 ppbv near 1500 m MSL, in all the profiles analyzed here..

The scatter between the individual 10-s TOPAZ profiles plotted in Fig. 3b increases rapidly with increasing range (R) from the lidar as the signal-to-noise ratio (SNR) of the backscatter return signals decreases due to ozone absorption, Rayleigh and Mie scattering, and the $1/R^2$ dependence of the lidar signals. The differences between the individual 10-s profiles increase to as much as 90 ppbv at 500 m MSL. The WP-3D in situ measurements show very little scatter, with differences of less than 4 ppbv across the 51 1-s samples; the standard deviation of the mean value is 0.8 ppbv. This is larger than the stated measurement precision of ± 0.05 ppbv, and likely represents the actual variability of ozone along the WP-3D flight path. This suggests that the large scatter in the TOPAZ measurements at low altitudes is mostly due to decreased measurement precision. This will be discussed in more detail below.

1) TOPAZ ACCURACY

The random scatter in the TOPAZ measurements is significantly improved by averaging multiple profiles, and the mean profile in Fig. 3b is much smoother than the individual profiles. The nearest TOPAZ range elements to the WP-3D altitude of 500 ± 8 m MSL are centered at 562 and 472 m MSL; the mean value at 517 m MSL is 83 ± 25 ppbv. This is $\sim 11\%$ lower than the mean value ($\pm 1 \sigma$) of 93.7 ± 0.8 ppbv from the in situ measurements. If we assume that the in situ measurements at ~ 500 m MSL are representative of the convectively well-mixed boundary layer, and extrapolate this value upward (short vertical dashed line in Fig. 3b), it intersects the mean TOPAZ profile at ~ 830 m MSL, which the backscatter profile shows is within the convectively well-mixed layer.

Figure 4 plots the data from Fig. 3b (on a different scale), along with similar plots for points G, H, and I. The mixed layer appears to be at least 700 m deep in all four cases. The scatter between the individual 10-s TOPAZ profiles at low altitudes is even greater at G (Fig. 4b), which has $\sim 40\%$ more column ozone. Thus the signals undergo more attenuation than at J (cf. Fig. 2a). Aerosol scattering and extinction also attenuate the signals, but to a much lesser degree. Indeed, there is $\sim 20\%$ less integrated backscatter in profile G than in J. The concentrations below ~ 800 m MSL in G are also significantly lower than both the in situ measurements and a nearby surface measurement from Katy Park (CAMS 559) represented by the orange star. There is considerably less scatter in the TOPAZ profiles and much better agreement with the in situ measurements at H (Fig. 4c) and I (Fig. 4d). Although this could be in part because the Twin Otter and WP-3D flight legs at H and I overlapped better, other factors appear to be more important. The

1σ statistical variability in the raw (10-s) profiles is only ~ 7 - 9 ppbv (6-10%) at ~ 1000 m MSL (~ 2300 m range) for all four points in Fig. 4, but ranges from ~ 11 to 27 ppbv (12-30%) at ~ 500 m MSL (~ 2800 m range).

Figure 5 shows scatter plots of the 10-s TOPAZ ozone mixing ratios measured at the center of each of the nine dashed boxes in Fig. 1a against the corresponding in situ measurements. The open circles represent points H and I, and the crossed circles G and J. Filled black circles represent the remaining points. The stars represent the coincident CAMS surface measurements where available. Figure 5 plots the TOPAZ data from the range gates nearest 500, 750, and 1000 m MSL against the WP-3D in situ measurements. The dashed and dotted lines represent the linear regression fits with the intercept left free and constrained to pass through the origin, respectively; the 1:1 line is solid. Both fits in Fig. 5a give slopes that are less than one, but the large scatter makes it difficult to estimate the measurement accuracy. The agreement is better in Fig 5b, and better yet in Fig. 5c, despite the fact that some of the 1000 m MSL measurements may lie above the top of the convectively well-mixed layer. Figure 6 is similar to Fig. 5, but now plots the (11 profile) TOPAZ and (51 point) in situ mean values for each point. The scatter in the TOPAZ measurements is reduced by a factor of about $\sqrt{11}$ revealing a systematic low bias at 500 m MSL compared to the in situ measurements. This bias is on the order of 10-15% for most of the averaged points, but less than 4% for points H and I. The agreement is much better at ~ 1000 m MSL, where the slope differs from unity by less than 1% with both free and fixed intercepts.

Table 1 summarizes the results from regression analyses of the TOPAZ profiles at center altitudes from 360 to 1525 m MSL. Only points separated by more than 450 m are

completely independent. The best agreement (within $\pm 2\%$) and highest degree of correlation is found between ~ 750 and 1000 m MSL. Although the SNR is higher above 1000 m MSL, worse agreement is found because the 450-m smoothed points included in the averages do not always lie entirely within in the convectively well-mixed layer. The correlation is weaker and the TOPAZ measurements systematically lower than the in situ measurements below 750 m MSL. The agreement actually improves slightly at the lowest altitudes as seen in Figs. 4a and 4b. This will be discussed below.

Figure 7 offers some insight into the TOPAZ negative bias at low altitudes. Figure 7a shows no systematic dependence of the TOPAZ/WP-3D ratio at 500 m MSL on the time delay between the two measurements within the 60 min window used here. Indeed, the five points with the smallest delays (± 30 min or less) have the greatest bias with an average ratio of 0.88 ± 0.03 . There is also no correlation between the ratio and aerosol mass and surface area determined by in situ instrumentation aboard the WP-3D (Parrish et al. 2009) (not shown). However, Fig. 7b shows that the TOPAZ/WP-3D ratio generally decreased when there was more ozone between the Twin Otter and 500 m MSL. This suggests a dependence on signal level (since more ozone means greater attenuation of the transmitted and received beams). This is confirmed in Fig. 7c, which plots the TOPAZ/WP-3D ratio directly as a function of SNR for the DIAL on line signal (i.e. the shortest and most strongly attenuated wavelength). The SNR is greater (and the agreement better) at H and I than at most of the other points. This is only partially due to less column ozone at H and I (cf. Fig. 7b); another factor was that the Twin Otter was flying at a lower altitude between H and I (cf. Fig. 1b) and a shorter range was required to

reach 500 m MSL. The range dependence accounts for the better agreement and lower scatter at point I (Fig. 4d) compared to point J (Fig. 4a) despite the profiles being similar.

b) TOPAZ PRECISION

Decreased SNR associated with high ozone columns and/or long range reduces the precision of the TOPAZ measurements. This is evident from the increased scatter between individual 10-s profiles (and the standard deviations of the mean profiles) plotted in Figs. 3 and 4. The nearly collocated measurements along the common H-I transect are consistent with these observations. Figure 8 plots time series of the WP-3D in situ ozone at 470 m MSL along this transect, along with the retrieved TOPAZ measurements from four different altitudes. The dashed lines show linear fits of the TOPAZ measurements. The mean TOPAZ ozone values at 964 (Fig. 8a) and 694 m MSL (Fig. 8b) are 2-4% higher than the mean in situ measurements, whereas the mean TOPAZ values at 458 and 334 m MSL are 7-8% lower. The standard deviation of the 335 1-s in situ measurements along the H-I transect is dominated by a smooth linear decrease of ~ 30 ppbv between H and I. When this trend is removed, the standard deviation of the in situ measurements decreases from 8 to 2 ppbv (2% of the mean) as shown by the histograms in Fig. 9a. This value is significantly larger than the stated in situ measurement precision of 0.05 ppbv and is believed to represent the atmospheric variability. The TOPAZ standard deviation of the 50 10-s profiles at 964 m MSL decreases from 12 to 8 ppbv (8% of the mean) when the trend is removed. The difference between the two measurements directly reflects the lower precision of the TOPAZ measurements. Figures 9b-9d show similar histogram plots for the time series plotted in

Figs. 8b-8d. The standard deviations increase to 18 ppbv (~20%) for the TOPAZ measurements below 500 m MSL.

Figure 10 summarizes these findings in a slightly different format. Figure 10a plots the standard deviations of the 11-profile means at four different altitude bins (~350, 500, 750, and 1000 m MSL) as a function of the SNR for the most strongly absorbed wavelength for G, H, I, and J. The solid line shows an exponential fit to the data. The standard deviation converges to ~8 ppbv when the SNR exceeds ~60. This value is still larger than the standard deviation of ~2 ppbv for the in situ measurements. Similar results are found when the 55 10-s measurements along the H-I transect are considered. The standard deviations of the de-trended transect data from Figs. 8 and 9 are plotted in Fig. 10b as a function of altitude instead of SNR. The standard deviation along this transect decreases exponentially, converging to ~4 ppbv at higher altitudes (i.e. shorter ranges). The decrease from ~8 to ~4 ppbv is consistent with the $\sqrt{5}$ increase in SNR due to the larger number of samples in the average. These results clearly show that the precision of the TOPAZ profiles depends directly on the SNR of the lidar return signals, which creates a dependence on both altitude and total ozone.

b. Low ozone: Dallas, 13 September

The flights near Dallas on 13 September provide an opportunity to evaluate TOPAZ under very different conditions. A trough over the Midwest brought relatively dry northerly flow with high background ozone levels over the Dallas area, but without the high static stability seen on 31 August. The potential for deep convection was moderate with a Lifted Index (a measure of the stability of the lower and middle

troposphere based on the temperature difference between a parcel lifted along the moist adiabat from the lifted condensation level (LCL) to 500 hPa) of -3.5 from the 0000 UTC Dallas sounding on 14 September. Surface heating was strong and the Dallas sounding indicated a convectively well-mixed layer up to ~1700 m MSL. Houston experienced a moderately high ozone day with maximum 8-h concentrations of up to 88 ppbv, but the 8-h concentrations in the Dallas area did not exceed 62 ppbv. This was the last flight of a six-week field deployment and the performance of TOPAZ was less than optimum: the solid-state laser was producing relatively low power, and the near-range channel was not operational. This restricted the useful operating range to 1575 to 2925 m below the aircraft or from ~1800 to 450 m MSL.

The two aircraft flew coordinated patterns to the south of the Dallas metropolitan area to intercept the urban plume. Figure 11 shows the Twin Otter and WP-3D flight tracks near Dallas. Both aircraft transected the plume three times as it was advected to the south by the almost northerly winds. Three long common transects are labeled in Fig. 11a. Both aircraft flew at constant altitudes during these transects (Fig. 11b), with time differences of 15 minutes or less for transects A and B, and 60 minutes or less for transect C. The WP-3D flew a fourth, parallel transect along the northern edge of Dallas. Figure 12 plots the WP-3D in situ measurements (red) at ~650 m MSL along transects A-C, together with the TOPAZ measurements at the 625 m MSL range gate (white). As shown in Fig. 11, the WP-3D flew further west in transect A, but the Twin Otter flew further west in transects B and C. The mean values along the sections with common measurements differ by ~1% for transects A and B, and ~5% for transect C, which has a greater time difference. Figure 13 is similar, but shows the TOPAZ measurements at 985

m MSL. The scatter is reduced by $\sim 35\%$ at the higher altitude. The mean values are 3-4% larger than those at 625 m MSL, but within $\sim 3\%$ of the in situ measurements. The good agreement is consistent with the findings from the 31 August measurements; the SNR at ~ 500 m MSL on 13 September was nearly double that measured on 31 August despite the lower laser power. This difference is largely due to the much lower aerosol and ozone (< 10 DU) loadings compared to those in the Houston area on 31 August.

The small differences between the TOPAZ results at 625 and 985 m MSL are consistent with the deep convective boundary layer over north central Texas on 13 September. Under these conditions, the precision of the TOPAZ measurements can be improved by additional vertical averaging. This is illustrated in Fig. 14 where the open white circles show the mean TOPAZ mixing ratios over the five range gates centered from 625 to 985 m MSL. Note that the vertical scales have been expanded compared to Figs. 12 and 13. The precision is improved and some of the fine structure seen in the in situ measurements is now visible in the TOPAZ measurements. This structure becomes even more pronounced when the data are horizontally smoothed as shown by the black points. These were obtained by applying a 11-point binomial (~ 6 km) smoothing window to the vertically integrated (625 to 985 m MSL) mean values. The smoothed TOPAZ data are in remarkable agreement ($\pm 2\%$) with the in situ measurements, particularly across transects A and B where the measurements are nearly coincident in time. The standard deviations of the vertically and horizontally averaged TOPAZ measurements are comparable to that of the in situ measurements, which are thought to reflect the ozone spatial variability. The good agreement shows that the errors associated with the ozone cross-sections and aerosol scattering corrections assumed in the DIAL

calculations (Alvarez et al. 2011) are very small. It also implies that most of the horizontal variations in ozone along these transects occurred on scales larger than 6 km. Notable exceptions are the sharp decreases along transect A not seen in the TOPAZ measurements where ozone has been titrated by fresh NO plumes from power plants south of Dallas.

4. Discussion and Conclusions

The measurements from TexAQS 2006 show that TOPAZ is capable of both high accuracy and good precision, but that both attributes depend on the return signal levels and hence total ozone, range, and spatial averaging. The 1σ statistical variability in the raw (10-s) profiles is ~7-9 ppbv (6-10%) at ~1000 m MSL and even less at higher altitudes and shorter ranges where the SNR is large (cf. Fig. 4). However, Fig. 5 shows that in many cases the individual profiles are not precise enough to substitute for in situ measurements below ~750 m MSL. The precision can be improved substantially beyond that of the individual 10-s profiles, however, with additional vertical and horizontal smoothing (cf. Fig. 14). Smoothed data are better suited for model inputs, satellite comparisons, or other applications that require less spatial resolution. The individual 10-s profiles are best suited for the creation of curtain plots such as those shown in Fig. 2, which have proven invaluable for the characterization of urban and power plant plumes.

A dependence of measurement precision on SNR, and hence range, is intrinsic to all DIAL measurements (Measures 1984). The dependence of TOPAZ measurement accuracy on SNR described here is unexpected, however. Like many other DIAL systems (Proffitt and Langford 1997), TOPAZ uses photomultiplier tubes operated in

current mode to detect the backscattered light. The resulting signals are then amplified and digitized. The signals can potentially be distorted by signal-induced bias (SIB) in the photomultiplier tubes (Zhao 1999), ringing or overshoot in the amplifiers (Rocadenbosch et al. 1998), or nonlinearities in the transient digitizers (Langford 1995). Any of these will degrade the accuracy of the retrieved concentrations.

The signal in the TOPAZ far range channel (Alvarez et al. 2011) decreases by more than a factor of 10^4 from the initial peak to the random noise level, which is typically dominated by photon statistics in the 1-s averages. The first analysis of the TexAQS 2006 data (version 1) gave unphysical ozone concentrations at low altitudes that were traced to amplifier overshoot comparable to the random noise level that distorted the signal baseline. An empirical procedure was used to correct this overshoot for version 2, but the present analysis suggests this correction is less than perfect and the signals are still slightly distorted at very low signal levels. The distortion decreases as the amplifier recovers, so that the retrieved concentrations near 350 m MSL are more accurate (but less precise) than the retrieved concentrations at 500 m MSL. Plots similar to Fig. 7c, but for different altitudes can also be used to derive empirical factors to correct the TOPAZ version 2 profiles. Figure 15 shows corrected (black) and uncorrected (blue) profiles for points G and J. The corrected profiles are in much better agreement with the in situ measurements and are relatively constant below ~ 1000 m MSL, consistent with the assumptions about the mixed layer depth. Laboratory tests are underway to better characterize this overshoot for future analyses.

Acknowledgements

The authors would like to thank Alan Brewer, Scott Sandberg, Richard Marchbanks, Brandi McCarty, Ann Weickmann, and Lisa Darby for their help with the TOPAZ instrumentation and data analysis during the TexAQS 2006 experiment. The authors would also like to acknowledge support from the NOAA Health of the Atmosphere program, the Texas Commission on Environmental Quality (under grant 582-8-86246), and the officers and crew of the NOAA Twin Otter and WP-3D.

References

- Alvarez, R. J., II, C. J. Senff, R. M. Hardesty, D. D. Parrish, W. T. Luke, T. B. Watson, P. H. Daum, and N. Gillani, 1998: Comparisons of airborne lidar measurements of ozone with airborne in situ measurements during the 1995 Southern Oxidants Study. *J. Geophys. Res.*, **103**, 31155-31171.
- Alvarez, R. J., II, C. J. Senff, A. O. Langford, A. M. Weickmann, D. C. Law, J. L. Machol, D. A. Merritt, R. D. Marchbanks, S. P. Sandberg, W. A. Brewer, R. M. Hardesty, and, R. M. Banta, 2011: Development and application of a compact tunable solid-state airborne ozone lidar system for boundary layer profiling. *J. Atmos. Oceanic Technol.*, submitted.
- Banta, R. M., C. J. Senff, A. B. White, M. Trainer, R. T. McNider, R. J. Valente, S. D. Mayor, R. J. Alvarez II, R. M. Hardesty, D. Parrish, and F. C. Fehsenfeld, 1998: Daytime buildup and nighttime transport of urban ozone in the boundary layer during a stagnation episode. *J. Geophys. Res.*, **103**, 22519-22544.
- Banta, R. M., C. J. Senff, J. Nielsen-Gammon, L. S. Darby, T. B. Ryerson, R. J. Alvarez, S. P. Sandberg, E. J. Williams, and M. Trainer, 2005: A bad air day in Houston. *Bull. Am. Meteorol. Soc.*, **86**, 657-669, doi:10.1175/BAMS-86-5-657.
- Banta, R. M., et al. 2011, Dependence of daily peak O₃ concentrations near Houston, Texas on environmental factors: Wind speed, temperature, and boundary-layer depth, *Atmos. Environ.*, **45**, 162-173.
- Browell, E. V., A. F. Carter, S. T. Shipley, R. J. Allen, C. F. Butler, M. N. Mayo, J. H. Siviter, Jr., and W. M. Hall, 1983: NASA multipurpose airborne DIAL system and measurements of ozone and aerosol profiles. *Appl. Opt.*, **22**, 522-534.

- Cooper, O. R., D. D. Parrish, A. Stohl, M. Trainer, P. Nedelec, V. Thouret, J. P. Cammas, S. J. Oltmans, B. J. Johnson, D. Tarasick, T. Leblanc, I. S. McDermid, D. Jaffe, R. Gao, J. Stith, T. Ryerson, K. Aikin, T. Campos, A. Weinheimer, and M. A. Avery, 2010: Increasing springtime ozone mixing ratios in the free troposphere over western North America. *Nature*, **463**, 344-348.
- Forster, P., V. Ramaswamy, P. Artaxo, T. Berntsen, R. Betts, D. W. Fahey, J. Haywood, J. Lean, D. C. Lowe, G. Myhre, J. Nganga, R. Prinn, G. Raga, S. M., and R. Van Dorland, 2007: Changes in atmospheric constituents and in radiative forcing. *Climate Change 2007: The Physical Science Basis. Contribution of Working Group I to the Fourth Assessment Report of the Intergovernmental Panel on Climate Change*, S. Solomon, D. Qin, M. Manning, Z. Chen, M. Marquis, K. B. Averyt, M. Tignor, and H. L. Miller, Eds., Cambridge Univ. Press.
- Forster, P. M. D., C. E. Johnson, K. S. Law, J. A. Pyle, and K. P. Shine, 1996: Further estimates of radiative forcing due to tropospheric ozone changes. *Geophysical Research Letters*, **23**, 3321-3324.
- Horowitz, L. W., 2006: Past, present, and future concentrations of tropospheric ozone and aerosols: Methodology, ozone evaluation, and sensitivity to aerosol wet removal. *J. Geophys. Res.*, **111**, doi:10.1029/2005JD006937.
- Kalnay, E., M. Kanamitsu, R. Kistler, W. Collins, D. Deaven, L. Gandin, M. Iredell, S. Saha, G. White, J. Woollen, Y. Zhu, M. Chelliah, W. Ebisuzaki, W. Higgins, J. Janowiak, K. C. Mo, C. Rolewski, J. Wang, A. Leetmaa, R. Reynolds, R. Jenne, and D. Joseph, 1996: The NCEP/NCAR 40-year reanalysis project. *Bull. Amer. Meteor. Soc.*, **77**, 437-471.

- Kleinman, L. I., P. H. Daum, D. G. Imre, Y.-N. Lee, L. J. Nunnermacker, S. R. Springston, J. Weinstein-Lloyd, and J. Rudolph, 2002: Ozone production rate and hydrocarbon reactivity in 5 urban areas: A cause of high ozone concentration in Houston. *Geophys. Res. Lett.*, **29**, 10.1029/2001GL014569.
- Kovalev, V. A. and J. L. McElroy, 1994: Differential Absorption Lidar Measurement of Vertical Ozone Profiles in the Troposphere That Contains Aerosol Layers with Strong Backscattering Gradients - a Simplified Version. *Appl. Opt.*, **33**, 8393-8401.
- Kuettner, J. P., P. A. Hildebrand, and T.L. Clark, 1987: Convection waves: observations of gravity wave systems over convectively active boundary layers, *Q. J. R. Meteorol. Soc.*, **113**, 445-487.
- Langford, A. O., 1995: Identification and correction of analog-to-digital converter nonlinearities and their implications for DIAL measurements. *Appl. Opt.*, **34**, 8330-8340.
- Langford, A. O. and S. J. Reid, 1998: Dissipation and mixing of a small-scale stratospheric intrusion in the upper troposphere. *J. Geophys. Res.*, **103**, 31265-31276.
- Langford, A. O., K. C. Aikin, C. S. Eubank, and E. J. Williams, 2009a: Stratospheric contribution to high surface ozone in Colorado during springtime,. *Geophys. Res. Lett.*, doi:10.1029/2009GL038367.
- Langford, A. O., C. J. Senff, R. M. Banta, R. M. Hardesty, R. J. Alvarez II, S. P. Sandberg, and L. S. Darby, 2009b: Regional and local background ozone in Houston during TexAQS 2006. *J. Geophys. Res.*, **114**, D00F12, doi:10.1029/2008JD011687.

- Langford, A. O., C. J. Senff, R. J. Alvarez, R. M. Banta, and R. M. Hardesty, 2010a: Long-range transport of ozone from the Los Angeles Basin: A case study. *Geophys. Res. Lett.*, **37**, L06807, doi:10.1029/2010GL042507.
- Langford, A. O., S. C. Tucker, C. J. Senff, R. M. Banta, W. A. Brewer, R. J. Alvarez, R. M. Hardesty, B. M. Lerner, and E. J. Williams, 2010b: Convective venting and surface ozone in Houston during TexAQS 2006. *J. Geophys. Res.*, **115**, doi 10.1029/2009jd013301.
- Machol, J. L., R. D. Marchbanks, C. J. Senff, B. J. McCarty, W. L. Eberhard, W. A. Brewer, R. A. Richter, R. J. Alvarez, D. C. Law, A. M. Weickmann, and S. P. Sandberg, 2009: Scanning tropospheric ozone and aerosol lidar with double-gated photomultipliers. *Appl. Opt.*, **48**, 512-524.
- Measures, R. M., 1984: *Laser remote sensing: fundamentals and applications*. Wiley-Interscience, 510 pp.
- Munro, R., R. Siddans, W. J. Reburn, and B. J. Kerridge, 1998: Direct measurements of tropospheric ozone distributions from space. *Nature*, **392**, 168-171.
- Newchurch, M. J., M. A. Ayoub, S. Oltmans, B. Johnson, and F. J. Schmidlin, 2003: Vertical distribution of ozone at four sites in the United States. *J. Geophys. Res.*, **108**, doi:10.1029/2002JD002059.
- Parrish, D. D., J. S. Holloway, M. Trainer, P. C. Murphy, G. L. Forbes, and F. C. Fehsenfeld, 1993: Export of North American ozone pollution to the North Atlantic Ocean. *Science*, **259**, 1436-1439.
- Parrish, D. D., D. T. Allen, T. S. Bates, M. Estes, F. C. Fehsenfeld, G. Feingold, R. Ferrare, R. M. Hardesty, J. F. Meagher, J. W. Nielsen-Gammon, R. B. Pierce, T. B.

- Ryerson, J. H. Seinfeld, and E. J. Williams, 2009: Overview of the Second Texas Air Quality Study (TexAQS II) and the Gulf of Mexico Atmospheric Composition and Climate Study (GoMACCS). *J. Geophys. Res.*, **114**, doi:10.1029/2009JD011842.
- Proffitt, M. H. and A. O. Langford, 1997: Ground-based differential absorption lidar system for day or night measurements of ozone throughout the free troposphere. *Appl. Opt.*, **36**, 2568-2585.
- Ridley, B. A., F. E. Grahek, and J. G. Walega, 1992: A small, high sensitivity, medium response ozone detector suitable for measurements from light aircraft. *J. Atmos. Oceanic Technol.*, **9**, 142-148.
- Rocadenbosch, F., A. Coméro, and D. Pineda, 1998: Assessment of lidar inversion errors for homogeneous atmospheres. *Appl. Opt.*, **37**, 2199-2206.
- Ryerson, T. B., M. P. Buhr, G. J. Frost, P. D. Goldan, J. S. Holloway, G. Hübler, B. T. Jobson, W. C. Kuster, S. A. McKeen, D. D. Parrish, J. M. Roberts, D. T. Sueper, M. Trainer, J. Williams, and F. C. Fehsenfeld, 1998: Emissions lifetimes and ozone formation in power plant plumes. *J. Geophys. Res.*, **103**, 22569-22583.
- Ryerson, T. B., M. Trainer, J. S. Holloway, D. D. Parrish, L. G. Huey, D. T. Sueper, G. J. Frost, S. G. Donnelly, S. Schauffler, E. L. Atlas, W. C. Kuster, P. D. Goldan, G. Hübler, J. F. Meagher, and F. C. Fehsenfeld, 2001: Observations of ozone formation in power plant plumes and implications for ozone control strategies. *Science*, **292**, 719-723.

- Senff, C. J., R. M. Hardesty, R. J. Alvarez II, and S. D. Mayor, 1998: Airborne lidar characterization of power plant plumes during the 1995 Southern Oxidants Study. *J. Geophys. Res.-Atmos.*, **103**, 31173-31189.
- Senff, C. J., R. J. Alvarez II, M. Hardesty, R. M. Banta, and A. O. Langford, 2010: Airborne lidar measurements of ozone flux downwind of Houston and Dallas. *J. Geophys. Res.*, **115**, D20307, doi:10.1029/2009JD013689.
- U.S. Environmental Protection Agency, 2006: Air quality criteria for ozone and related photochemical oxidants, v. I-III EPA 600/R-05/004bF.
- White, A. B., C. J. Senff, and R. M. Banta, 1999: A comparison of mixing depths observed by ground-based wind profilers and an airborne lidar, *J. Atmos. Oceanic Technol.*, **16**, 584-590.
- Zhao, Y. Z., 1999: Signal-induced fluorescence in photomultipliers in differential absorption lidar systems. *Appl. Opt.*, **38**, 4639-4648.

Figure Captions

Fig. 1. (a) Map of the greater Houston area showing flight tracks of the NOAA Twin Otter (blue) and WP-3D (red) on the afternoon of 31 August 2006. The urban areas are colored yellow. The contours show surface ozone values from the TCEQ CAMS network at 2100 UT. The dashed squares enclose the comparison points, which are identified by black letters (the gray letters denote intersections where the time difference was greater than 60 minutes). The dotted boxes enclose the GJ and HI transects. The orange circles represent the nearest CAMS stations to each of the comparison points that lie within the dashed squares. (b) Flight altitudes of the Twin Otter (blue) and WP-3D (red) on 31 August.

Fig. 2. (a) Curtain plot of ozone mixing ratios from the 10-s TOPAZ profiles within the dotted rectangle enclosing the northbound flight leg from J to G in Fig. 1a. The open squares show the in situ measurements from the WP-3D. (b) Same as (a), but for the southbound flight leg from H to I. The solid black line shows the altitude of the peak gradient in aerosol backscatter identified using a Haar wavelet technique.

Fig. 3. (a) Detailed map of the area surrounding point J from Fig. 1a. The dashed box encloses a 6 x 6 km square with 11 10-s TOPAZ measurements (blue squares) and 51 1-s in situ measurements from the WP-3D (overlapping red squares). (b) Ozone and aerosol profiles measured within box J. The dotted blue lines represent the 10-s ozone profiles and the heavy black line the mean ($\pm 1\sigma$) of those profiles. The green line shows the corresponding mean aerosol backscatter profile and the red squares the in situ ozone

measurements. The dotted horizontal and dashed vertical black lines represent the minimum mixed layer depth estimated from the aerosol backscatter profile. The heavy dashed blue line shows the ozone error due to aerosol scattering.

Fig. 4. TOPAZ and in situ measurements from points G, H, I, and J plotted on a common scale. The colors and symbols are the same as in Fig. 3. The mean TOPAZ values ($\pm 1\sigma$) at ~500 and 750 m MSL are shown, as is the time difference between the TOPAZ and in-situ measurements. The orange stars in (b) represents the 5-min ozone concentrations measured at CAMS 559 (Katy Park) during the Twin Otter (132.6 ppbv) and WP-3D (130.1 ppbv) overpasses.

Fig. 5. Scatter plots of TOPAZ and WP-3D in situ measurements from the center points of the dashed boxes in Fig. 1a near (a) 500 and (b) 750 m, and (c) 1000 MSL. The open circles represent points H and I, and the circled crosses G and J. The remaining points are represented by filled circles. The stars denote nearby CAMS measurements. The 1:1 line is solid; the dashed and dotted lines show the parameters ($\pm 1\sigma$) from linear regressions with free and fixed intercepts, respectively.

Fig. 6. Scatter plots of the 11-point mean TOPAZ and WP-3D in situ measurements from the dashed boxes in Fig. 1 near (a) 500, (b) 750, and (c) 1000 m MSL. The symbols are the same as in Fig. 5. The error bars show the standard deviation of the mean. The 1:1 is solid and the dashed and dotted lines show the parameters ($\pm 1\sigma$) from linear

regressions with free and fixed intercepts, respectively. The CAMS data are omitted for clarity.

Fig. 7. Ratio of the mean TOPAZ and in situ measurements from Fig. 6a plotted as a function of (a) time difference, (b) total ozone (in Dobson Units, DU) below the Twin Otter, and (c) SNR of the far channel on line (288 nm) signal. The symbols are the same as in Fig. 5. The $\pm 20\%$ limits are represented by the dotted lines.

Fig. 8. TOPAZ (white) and in situ (red) ozone mixing ratios along the flight leg from H to I in Fig. 1a. The TOPAZ data are plotted for range gates near (a) 1000, (b) 700, (c) 500, and (d) 300 m MSL. The dashed lines represent the linear fits to the TOPAZ measurements. The mean values ($\pm 1\sigma$) are indicated.

Fig. 9. Histograms of the de-trended TOPAZ (gray) and in situ (red) ozone distributions measured along the H-I flight leg and the mean value $\pm 1\sigma$. The TOPAZ measurements are shown for the same four altitudes as in Fig. 8.

Fig. 10. Standard deviation of the TOPAZ measurements calculated from (a) mean profiles for points G, H, I, and J (11 10-s averages) at the four altitudes from Fig. 9, plotted as a function of the far channel on line SNR. The open circles represent points H and I, and the circled crosses show points G and J. The solid line shows an exponential fit to the data. (b) De-trended measurements from the H-I transect (55 10-s averages)

plotted as a function of altitude. The dashed line shows the corresponding standard deviation of the in situ measurements. The solid line shows an exponential fit to the data.

Fig. 11. Map of the greater Dallas area showing the Twin Otter (blue) and WP-3D (red) flight tracks on 13 September 2006. The red squares show the points along transects A, B, and C where there were common measurements. (b) Flight altitudes of the Twin Otter (blue) and WP-3D (red) during the common measurements.

Fig. 12. TOPAZ (white) and in situ (red) ozone measurements at 625 and 650 m MSL, respectively, from transects A, B, and C. The means and standard deviations along the common points are also shown.

Fig. 13. TOPAZ (white) and in situ (red) ozone measurements at 985 and 650 m MSL, respectively, from transects A, B, and C. The means and standard deviations along the common points are also shown.

Fig. 14. TOPAZ and in situ (red) ozone measurements from transects A, B, and C. The TOPAZ measurements are averaged over the column from 625 to 985 m MSL with (black) and without (white) 11-point horizontal smoothing. The means and standard deviations along the common points are also shown. Note that the vertical scales have been expanded compared to Figs. 12 and 13.

Fig. 15. Corrected (black) and uncorrected (blue) ozone profiles from profiles (a) G and (b) J from 31 August. The plotted profiles are the averages of the 11 10-s profiles within the dashed boxes of Fig. 1a. The red squares show the 1-s WP-3D in situ measurements.

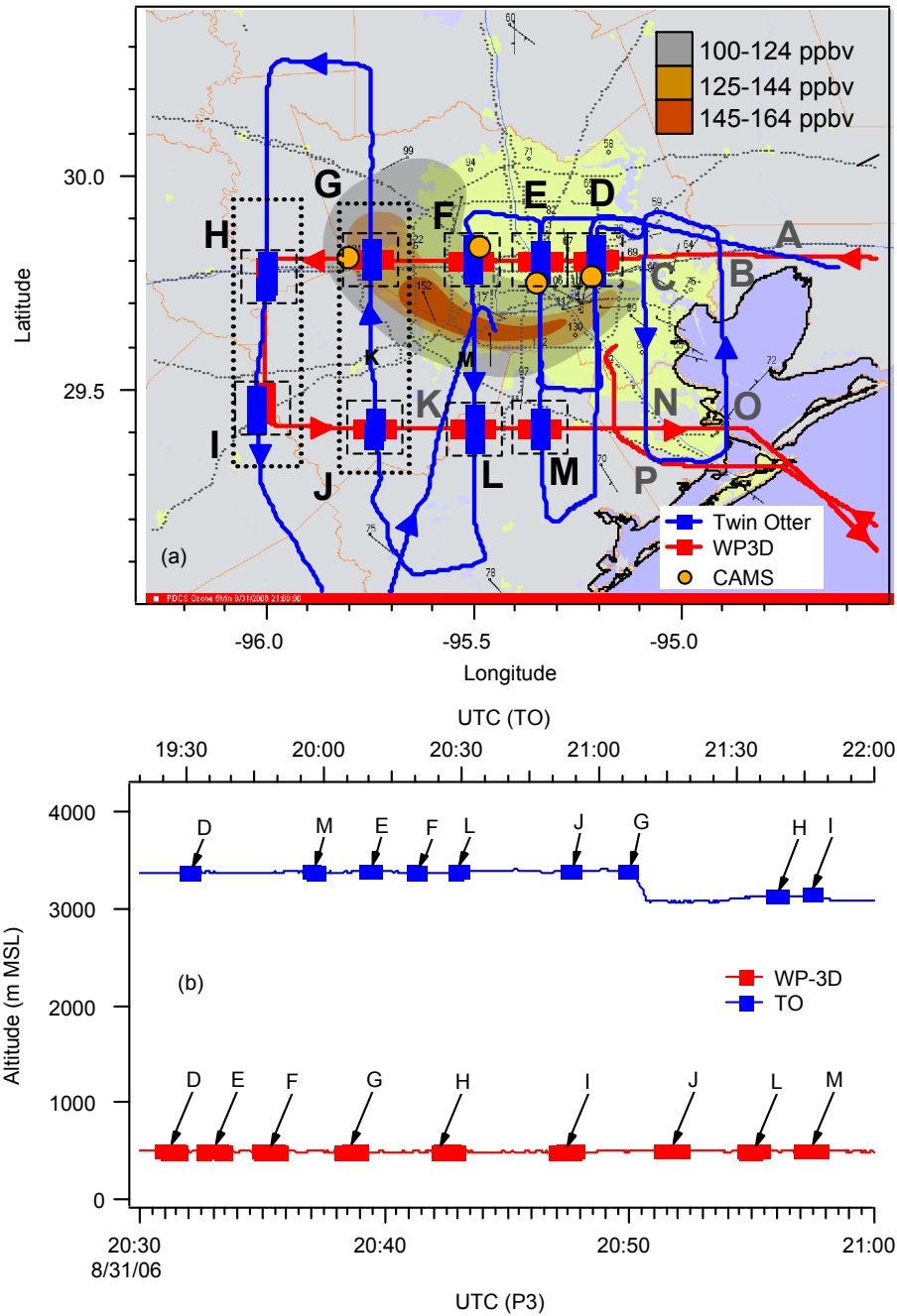


Fig. 1. (a) Map of the greater Houston area showing flight tracks of the NOAA Twin Otter (blue) and WP-3D (red) on the afternoon of 31 August 2006. The urban areas are colored yellow. The contours show surface ozone values from the TCEQ CAMS network at 2100 UT. The dashed squares enclose the comparison points, which are identified by black letters (the gray letters denote intersections where the time difference was greater than 60 minutes). The dotted boxes enclose the GJ and HI transects. The orange circles represent the nearest CAMS stations to each of the comparison points that lie within the dashed squares. (b) Flight altitudes of the Twin Otter (blue) and WP-3D (red) on 31 August.

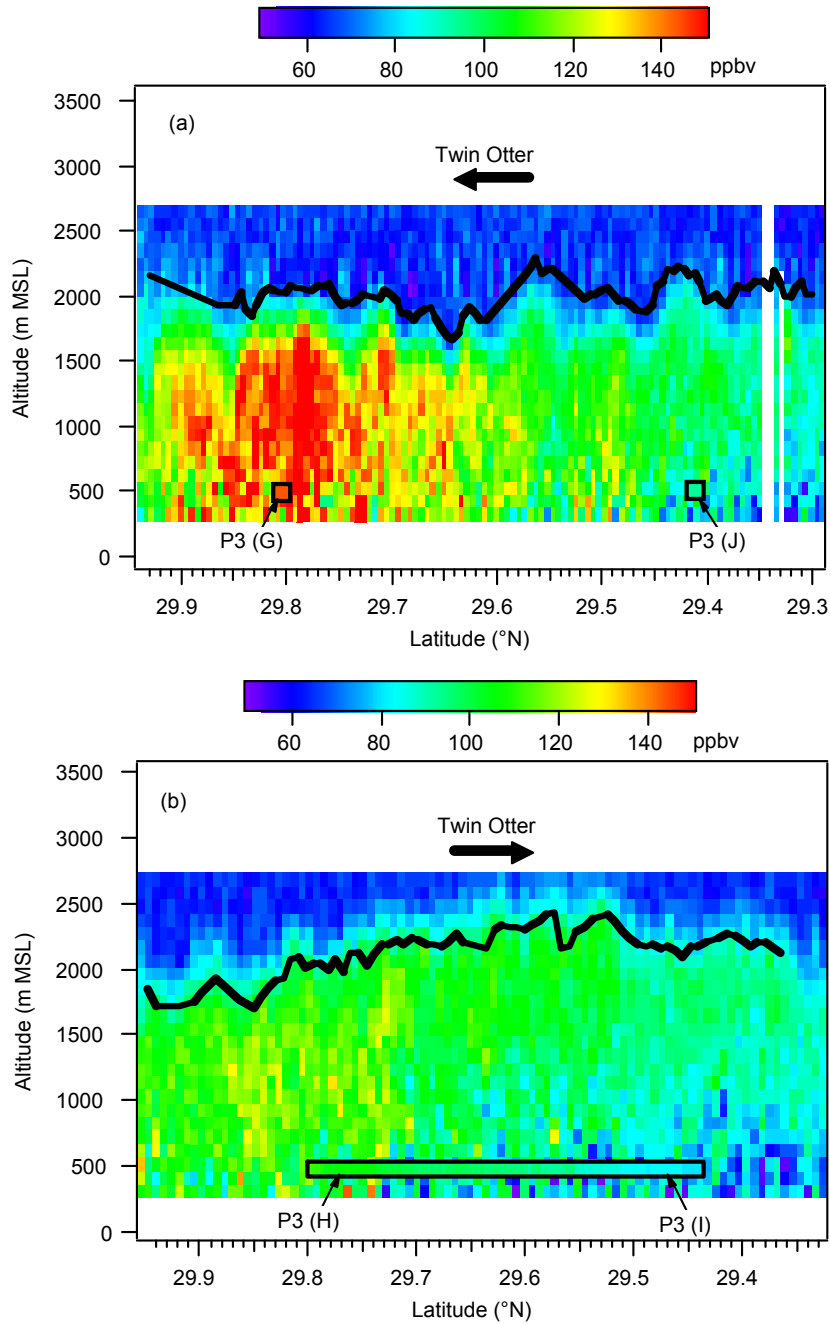


Fig. 2. (a) Curtain plot of ozone mixing ratios from the 10-s TOPAZ profiles within the dotted rectangle enclosing the northbound flight leg from J to G in Fig. 1a. The open squares show the in situ measurements from the WP-3D. (b) Same as (a), but for the southbound flight leg from H to I. The solid black line shows the altitude of the peak gradient in aerosol backscatter identified using a Haar wavelet technique.

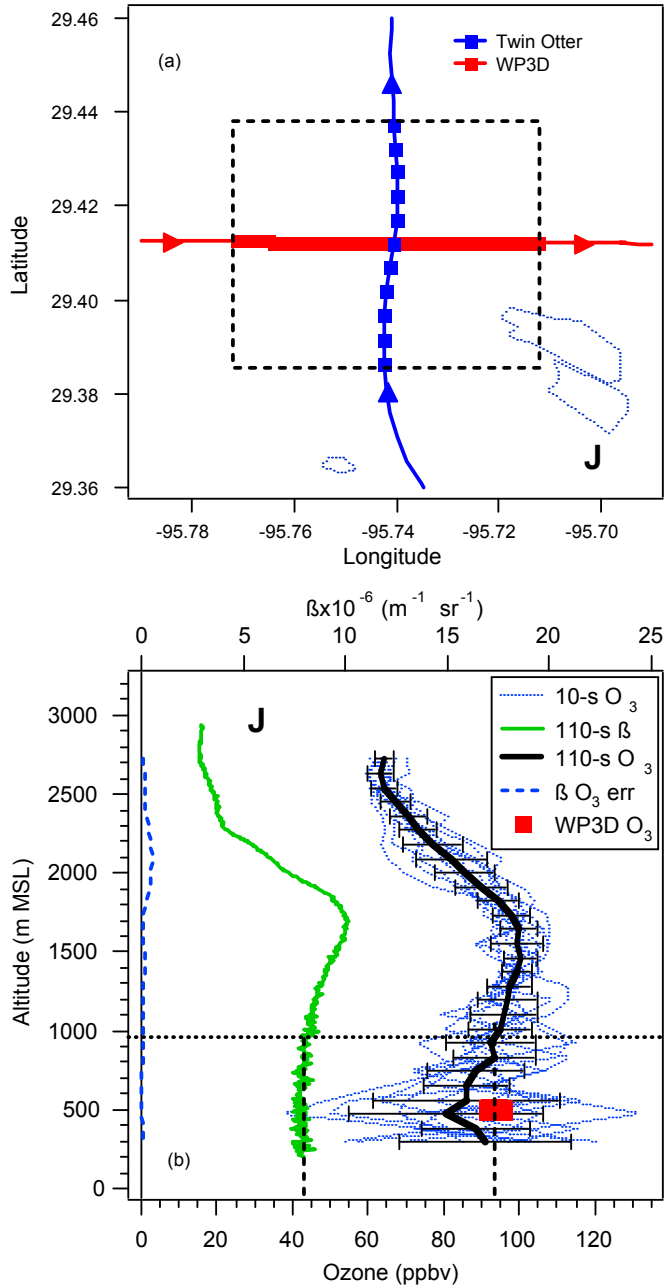


Fig. 3. (a) Detailed map of the area surrounding point J from Fig. 1a. The dashed box encloses a 6 x 6 km square with 11 10-s TOPAZ measurements (blue squares) and 51 1-s in situ measurements from the WP-3D (overlapping red squares). (b) Ozone and aerosol profiles measured within box J. The dotted blue lines represent the 10-s ozone profiles and the heavy black line the mean ($\pm 1\sigma$) of those profiles. The green line shows the corresponding mean aerosol backscatter profile and the red squares the in situ ozone measurements. The dotted horizontal and dashed vertical black lines represent the minimum mixed layer depth estimated from the aerosol backscatter profile. The heavy dashed blue line shows the ozone error due to aerosol scattering.

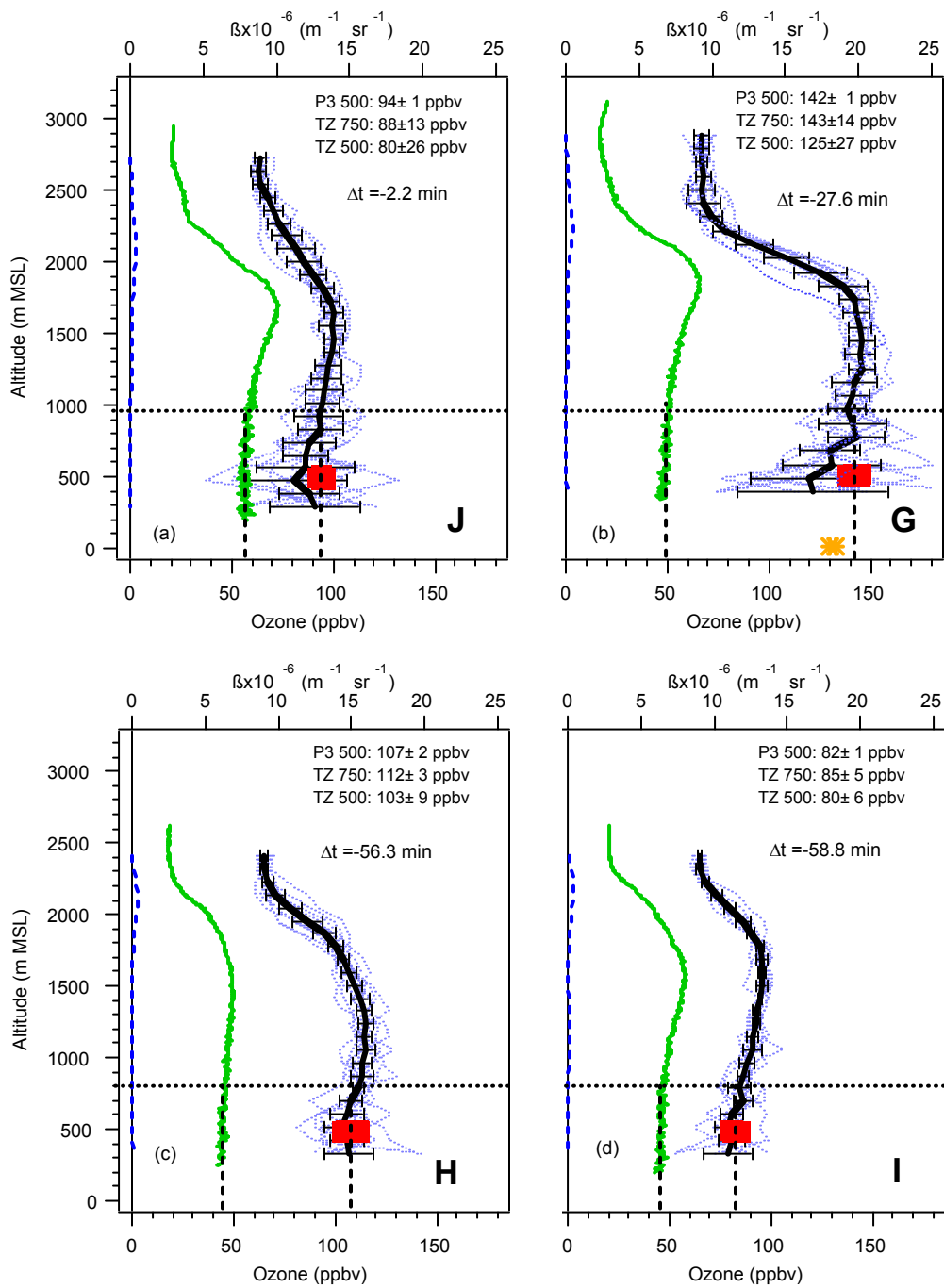


Fig. 4. TOPAZ and in situ measurements from points G, H, I, and J plotted on a common scale. The colors and symbols are the same as in Fig. 3. The mean TOPAZ values ($\pm 1\sigma$) at ~ 500 and 750 m MSL are shown as is the time difference between the TOPAZ and in-situ measurements. The orange stars in (b) represents the 5-min ozone concentrations measured at CAMS 559 (Katy Park) during the Twin Otter (132.6 ppbv) and WP-3D (130.1 ppbv) overpasses.

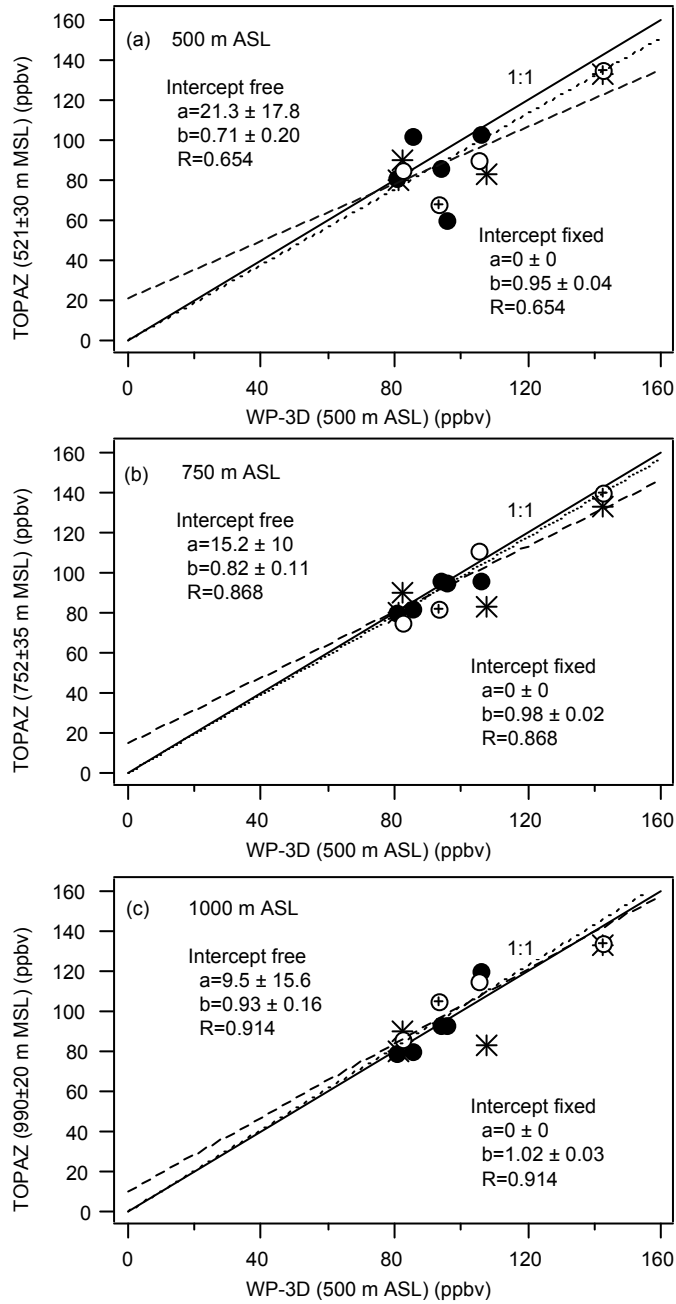


Fig. 5. Scatter plots of TOPAZ and WP-3D in situ measurements from the center points of the dashed boxes in Fig. 1a near (a) 500 and (b) 750 m, and (c) 1000 MSL. The open circles represent points H and I, and the circled crosses G and J. The remaining points are represented by filled circles. The stars denote nearby CAMS measurements. The 1:1 line is solid; the dashed and dotted lines show the parameters ($\pm 1\sigma$) from linear regressions with free and fixed intercepts, respectively.

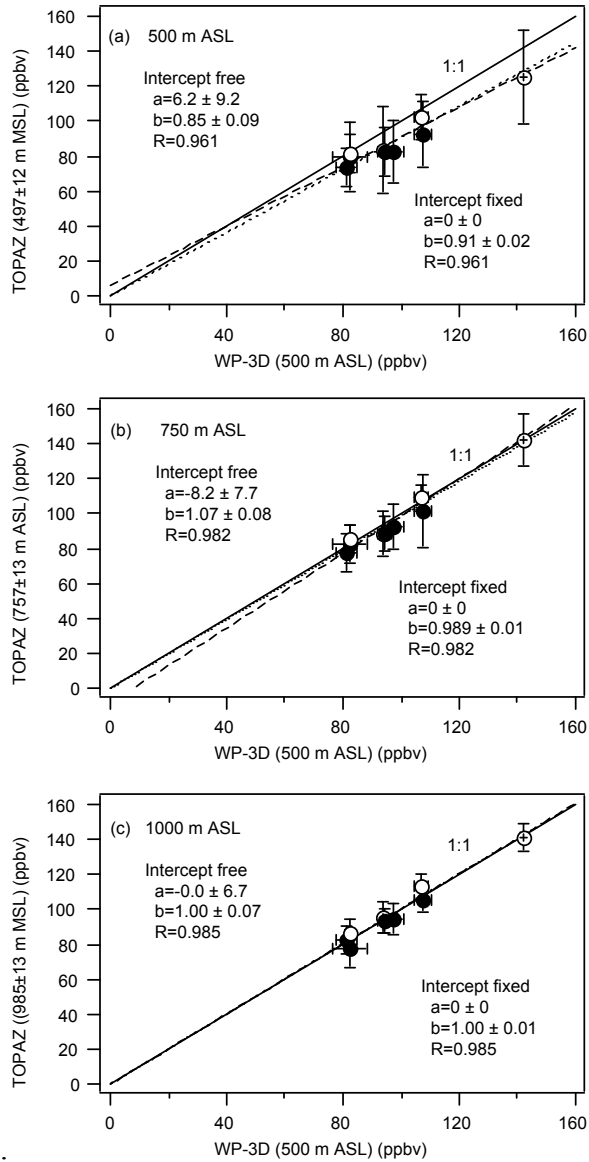


Fig. 6. Scatter plots of the 11-point mean TOPAZ and WP-3D in situ measurements from the dashed boxes in Fig. 1 near (a) 500, (b) 750, and (c) 1000 m MSL. The symbols are the same as in Fig. 5. The error bars show the standard deviation of the mean. The 1:1 is solid and the dashed and dotted lines show the parameters ($\pm 1\sigma$) from linear regressions with free and fixed intercepts, respectively. The CAMS data are omitted for clarity.

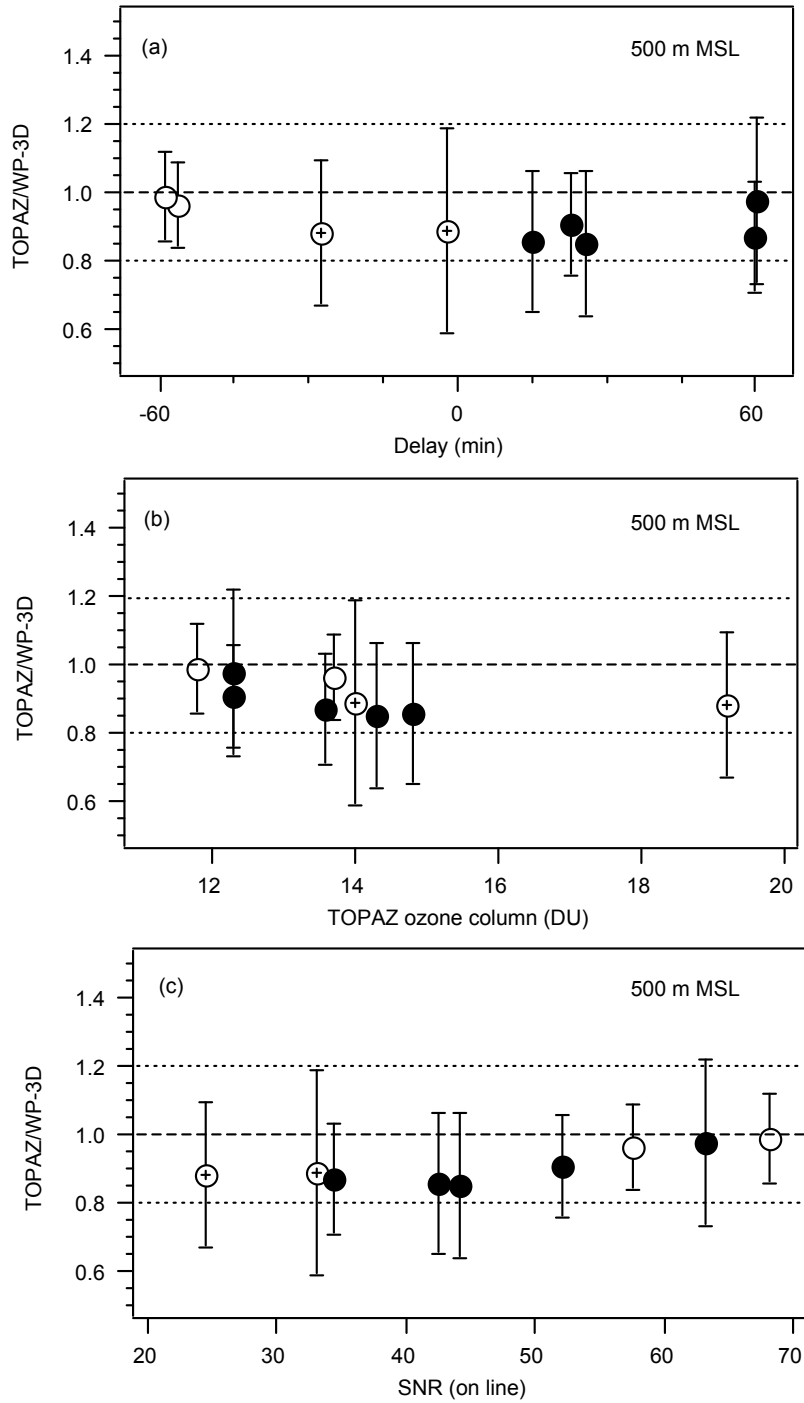


Fig. 7. Ratio of the mean TOPAZ and in situ measurements from Fig. 6a plotted as a function of (a) time difference, (b) total ozone (in Dobson Units, DU) below the Twin Otter, and (c) SNR of the far channel on line (288 nm) signal. The symbols are the same as in Fig. 5. The $\pm 20\%$ limits are represented by the dotted lines.

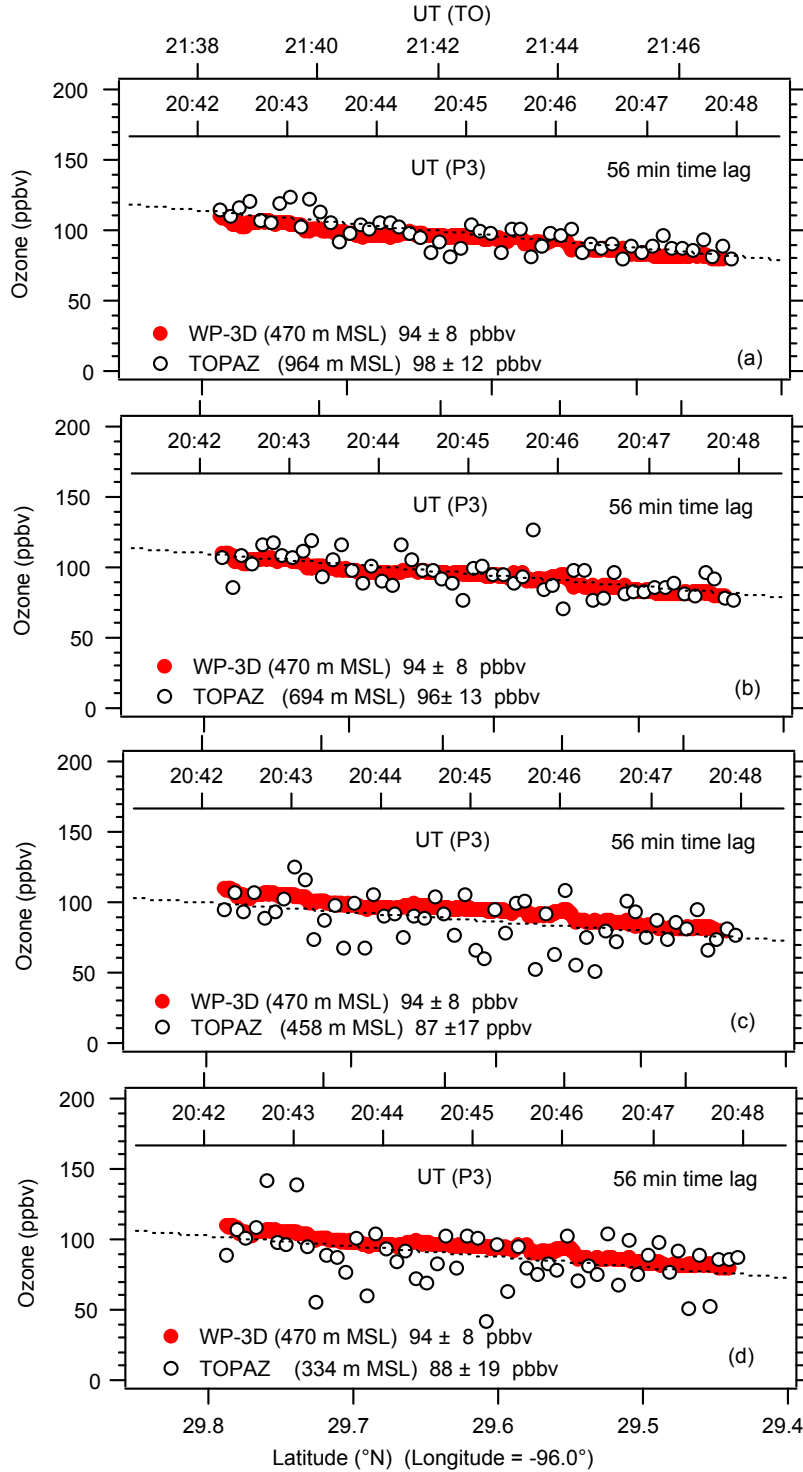


Fig. 8. TOPAZ (white) and in situ (red) ozone mixing ratios along the flight leg from H to I in Fig. 1a. The TOPAZ data are plotted for range gates near (a) 1000, (b) 700, (c) 500, and (d) 300 m MSL. The dashed lines represent the linear fits to the TOPAZ measurements. The mean values ($\pm 1\sigma$) are indicated.

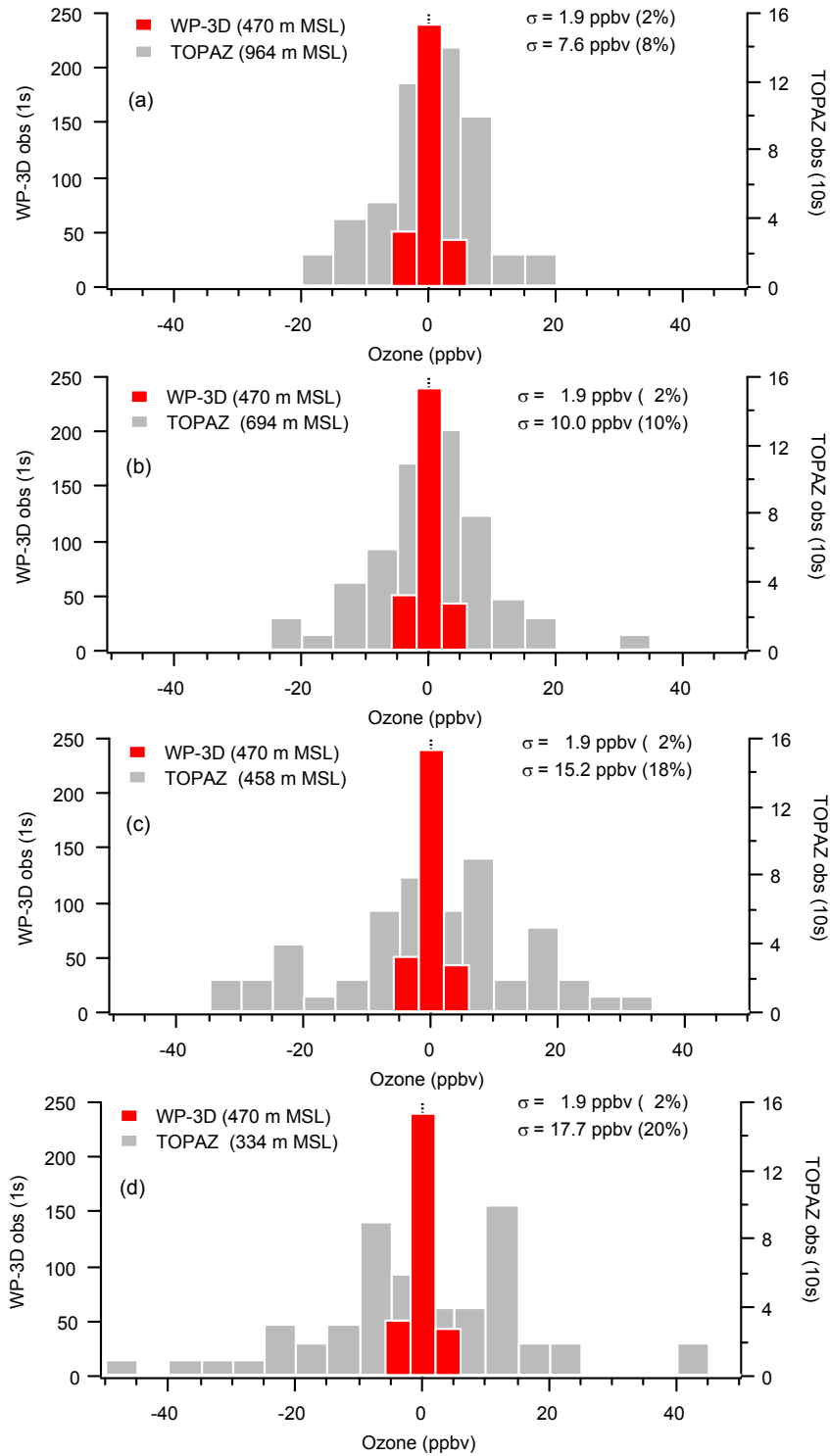


Fig. 9. Histograms of the de-trended TOPAZ (gray) and in situ (red) ozone distributions measured along the H-I flight leg and the mean value $\pm 1\sigma$. The TOPAZ measurements are shown for the same four altitudes as in Fig. 8.

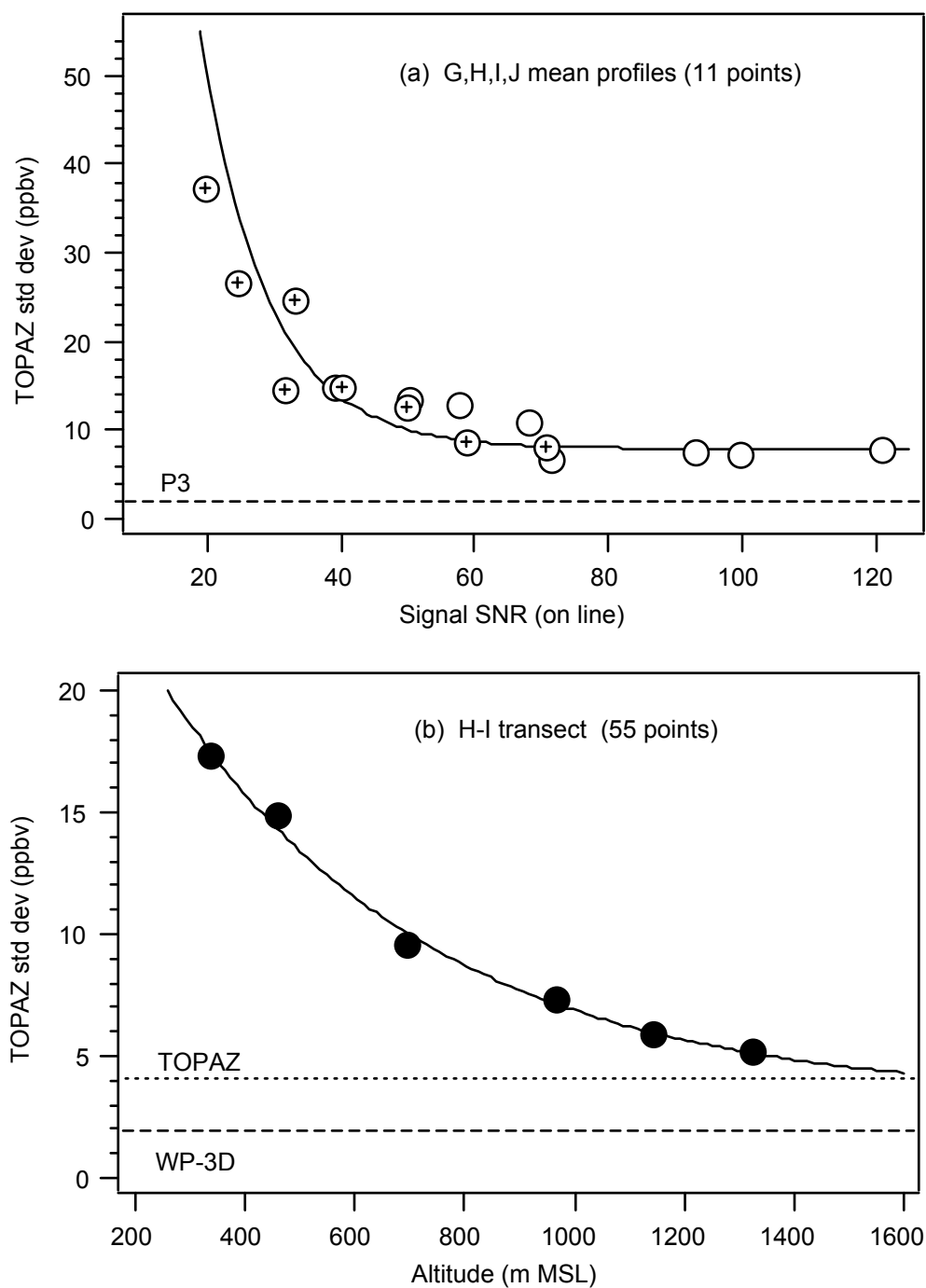


Fig. 10. Standard deviation of the TOPAZ measurements calculated from (a) mean profiles for points G, H, I, and J (11 10-s averages) at the four altitudes from Fig. 9, plotted as a function of the far channel on line SNR. The open circles represent points H and I, and the circled crosses show points G and J. The solid line shows an exponential fit to the data. (b) De-trended measurements from the H-I transect (55 10-s averages) plotted as a function of altitude. The dashed line shows the corresponding standard deviation of the in situ measurements. The solid line shows an exponential fit to the data.

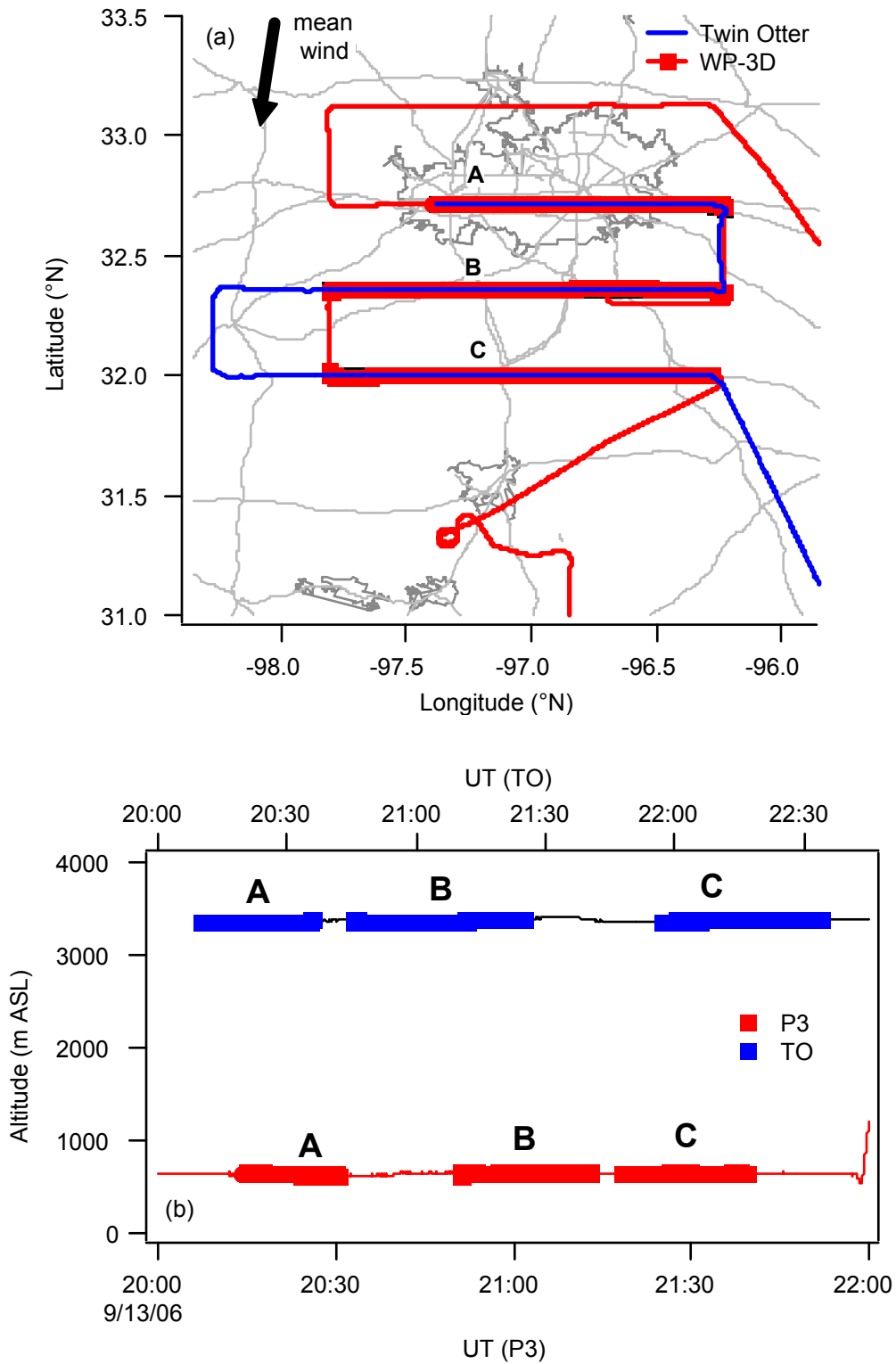


Fig. 11. Map of the greater Dallas area showing the Twin Otter (blue) and WP-3D (red) flight tracks on 13 September 2006. The red squares show the points along transects A, B, and C where there were common measurements. (b) Flight altitudes of the Twin Otter (blue) and WP-3D (red) during the common measurements.

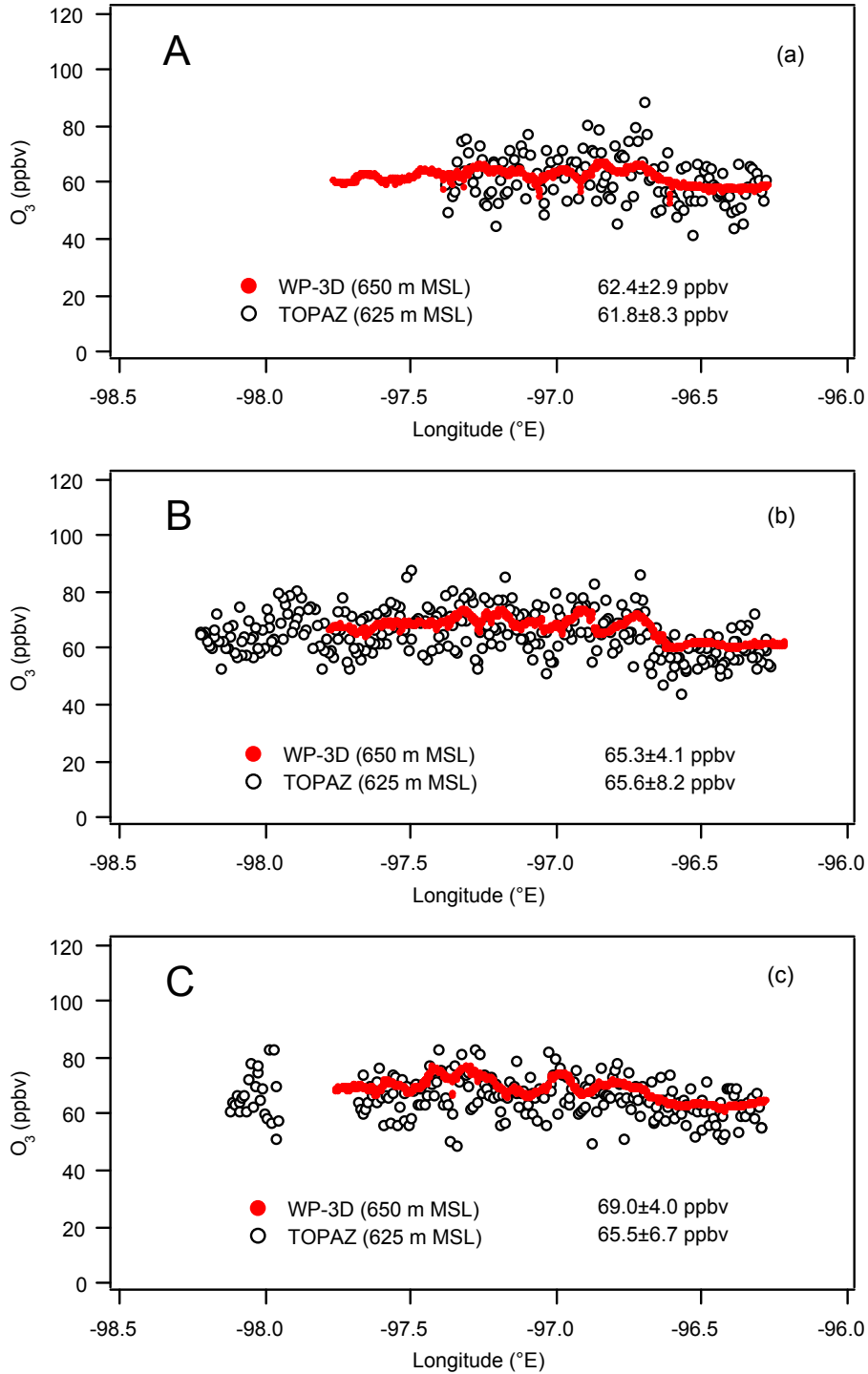


Fig. 12. TOPAZ (white) and in situ (red) ozone measurements at 625 and 650 m MSL, respectively, from transects A, B, and C. The means and standard deviations along the common points are also shown.

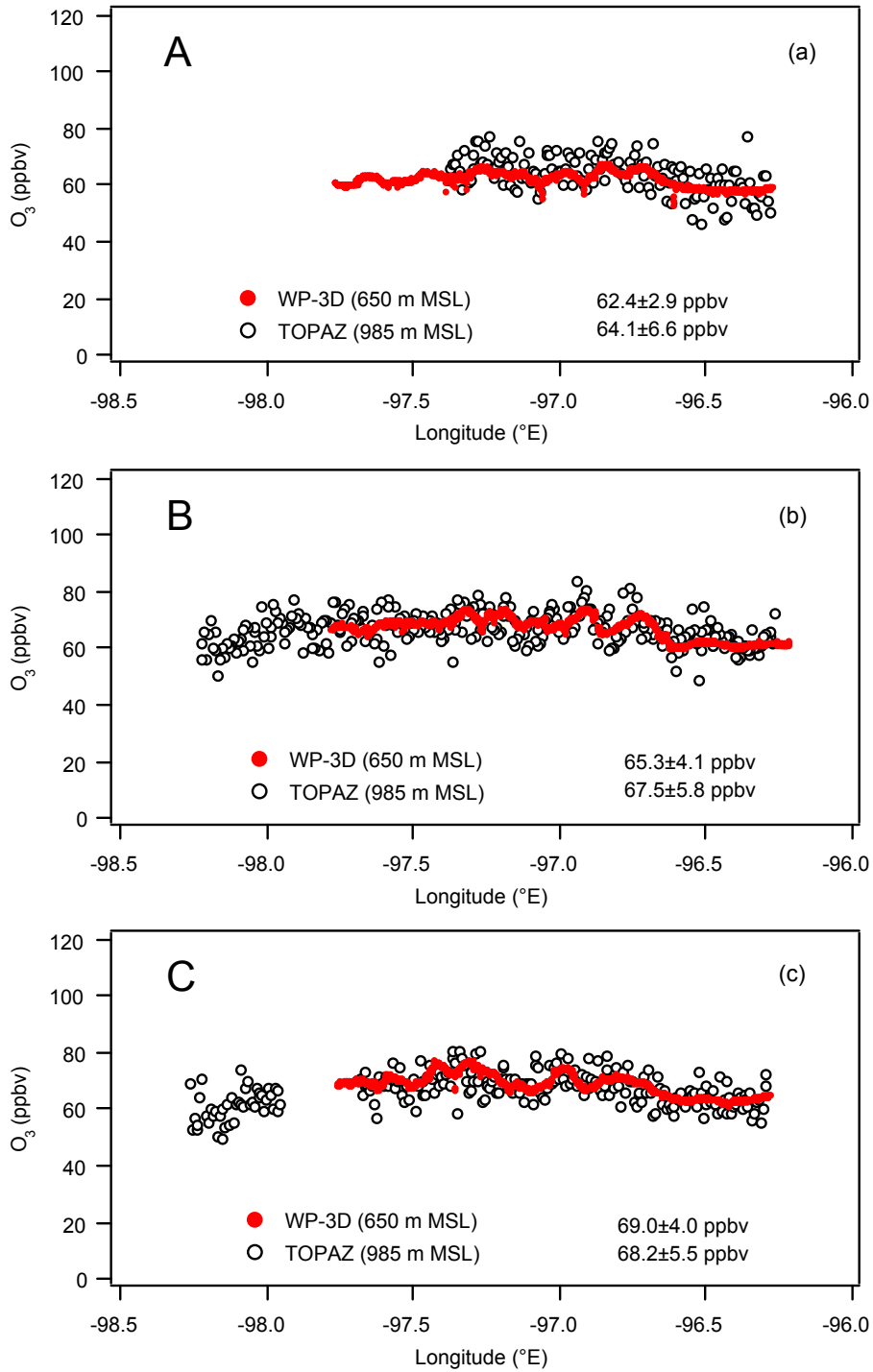


Fig. 13. TOPAZ (white) and in situ (red) ozone measurements at 985 and 650 m MSL, respectively, from transects A, B, and C. The means and standard deviations along the common points are also shown.

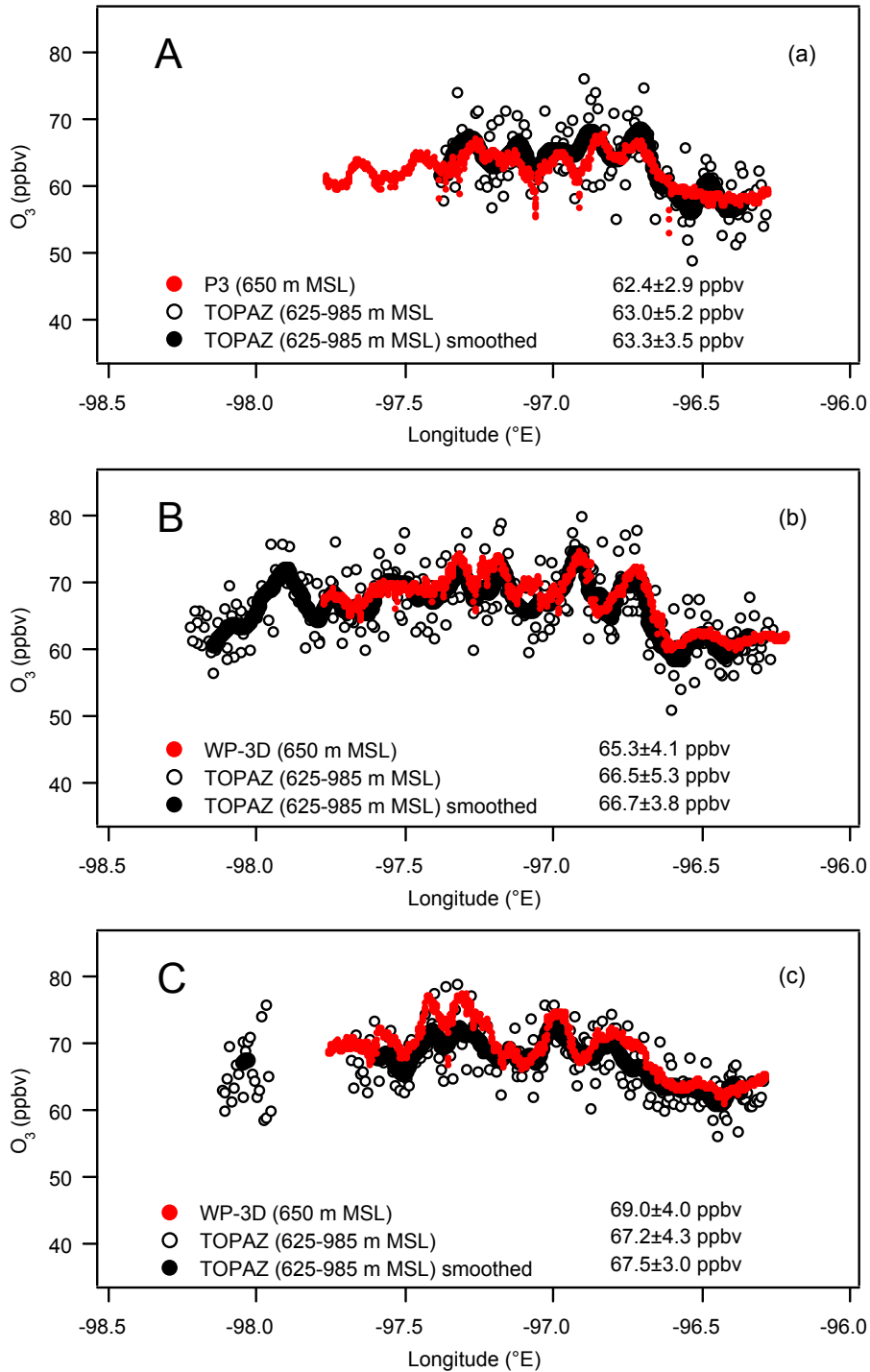


Fig. 14. TOPAZ and in situ (red) ozone measurements from transects A, B, and C. The TOPAZ measurements are averaged over the column from 625 to 985 m MSL with (black) and without (white) 11-point horizontal smoothing. The means and standard deviations along the common points are also shown. Note that the vertical scales have been expanded compared to Figs. 12 and 13.

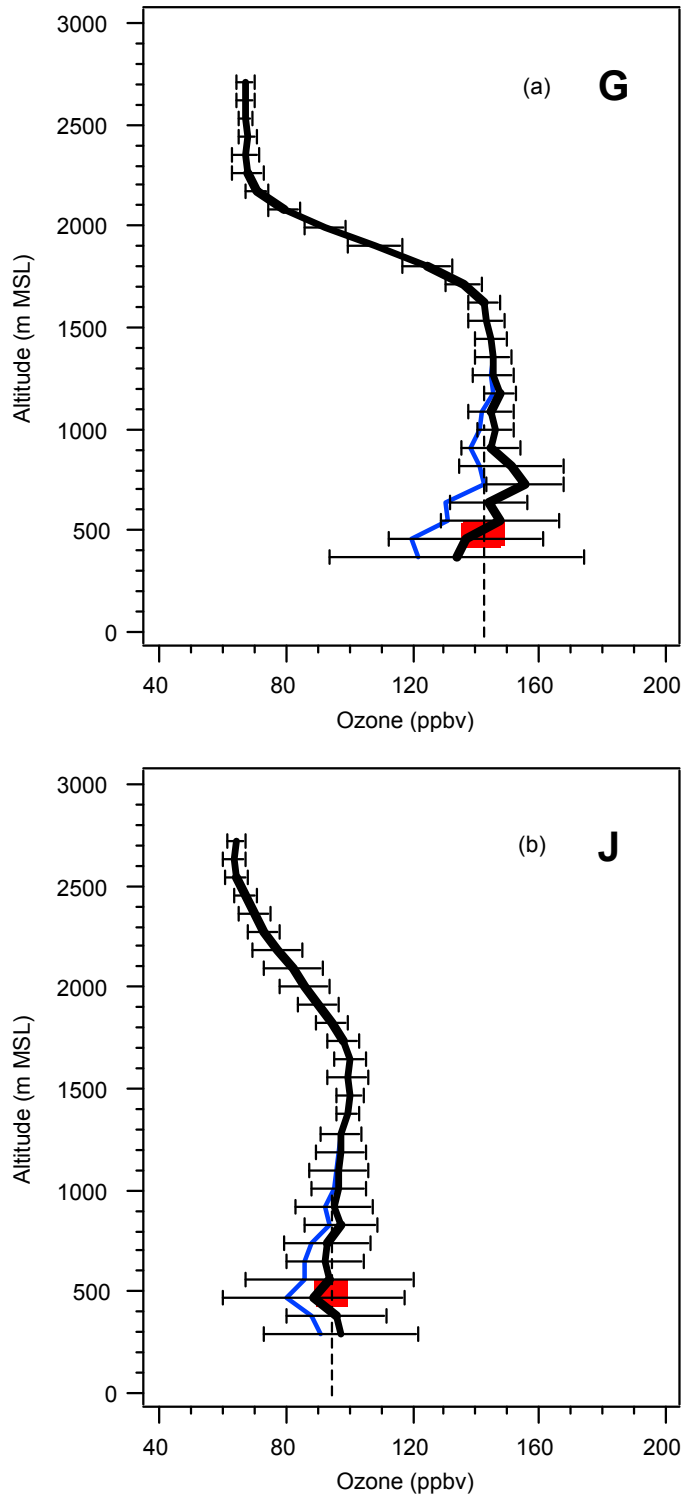


Fig. 15. Corrected (black) and uncorrected (blue) ozone profiles from profiles (a) G and (b) J from 31 August. The plotted profiles are the averages of the 11 10-s profiles within the dashed boxes of Fig. 1a. The red squares show the 1-s WP-3D in situ measurements.

Table 1. Linear regression of 31 August 10-s averages with in situ measurements .

Z (m MSL)*	intercept ($\pm\sigma$)	slope ($\pm\sigma$)	fixed slope ($\pm\sigma$)	R ²
360	-4.9±10.7	0.97±0.11	0.92±0.02	0.923
500	6.2±9.2	0.85±0.09	0.91±0.02	0.925
625	-4.0±7.0	0.98±0.07	0.94±0.01	0.966
750	-8.2±7.7	1.07±0.08	0.99±0.01	0.965
800	-9.5±7.3	1.09±0.10	1.00±0.01	0.975
985	-0.0±6.7	1.00±0.07	1.00±0.01	0.970
1125‡	-3.2±8.1	1.06±0.08	1.03±0.01	0.961
1250‡	2.9±7.1	1.03±0.07	1.06±0.01	0.968
1525‡	13.8±15.5	0.93±0.16	1.07±0.03	0.839

* approximate center point of 5-point (450-m m) smoothed profiles. The actual center point changes slightly with the Twin Otter altitude.

‡ these entries are influenced by data that lie above the mixed layer.